Angular dependence of phonon transmission through a Fibonacci superlattice

D. C. Hurley, S. Tamura,* and J. P. Wolfe
Department of Physics and Materials Research Laboratory, University of Illinois at Urbana-Champaign, 104 South Goodwin Avenue, Urbana, Illinois 61801

K. Ploog and J. Nagle
Max-Planck-Institut für Festkörperphysik, Heisenbergstrasse 1, Postfach 80 06 65, D-7000 Stuttgart 80, Federal Republic of Germany
(Received 16 October 1987)

Phonon imaging is employed to examine the propagation of acoustic phonons through a Fibonacci superlattice. Ballistic transmission of phonons with $\nu > 850$ GHz through 750 superlattice interfaces is detected. In addition, sharp variations in the phonon intensity with propagation angle are observed. These measurements are consistent with Monte Carlo simulations presented in this paper. Distinct stop bands are expected theoretically, and the angular dependence of these structures is remarkably similar to those predicted for a periodic superlattice.

I. INTRODUCTION

The recent discovery of metallic alloys exhibiting icosohedral crystallographic symmetry[1] was one of the most surprising in modern condensed-matter physics. Theoretical studies of the materials[2] soon revealed that their properties could be explained neither by a periodic array of atoms nor a totally random placement. The materials belonged to a third, totally new class of materials—*quasiperiodic* crystals. Since the initial discovery in 1984, the properties of one-, two-, and three-dimensional quasiperiodic systems, including their vibrational properties,[3–8] have been examined. In one dimension, arrays ordered according to the Fibonacci series display quasiperiodic characteristics. In 1985, Merlin *et al.*[9] fabricated a Fibonacci superlattice (SL), i.e., a SL which the individual AlAs/GaAs layers alternate according to a Fibonacci (iteration) rule. Subsequent x-ray[10] studies revealed that this heterostructure indeed exhibited properties characteristic of quasiperiodic systems. Raman experiments[11] have been performed on similar Si/Ge superlattices.

The acoustic-phonon propagation through *periodic* SL's is a highly complex yet interesting process, and has recently been the subject of experimental[12–15] and theoretical research.[16–19] Bragg scattering of acoustic phonons has been observed in several crystalline[12,14] and amorphous[13,15] systems. Basically, gaps in the phonon frequency ("stop bands") occur when the phonon wave vector touches the boundary of the Brillouin zone. Corresponding dips in transmission have been observed by phonon-spectroscopy and phonon-imaging techniques. Elastic anisotropies make this a particularly interesting problem. It is found, for example, that coupling between the longitudinal (L) and fast and slow transverse (FT and ST) phonon modes at an interface produces a new type of "coupled-mode stop band" which occurs *inside* the Brillouin zone.[19] Such intrazone stop bands occur only for phonons incident on the SL at oblique angles.

In this paper, we will examine the transmission of short-wavelength acoustic phonons through a quasiperiodic SL. The theoretical basis for this problem has been previously reported by Tamura and Wolfe.[8] Well-defined stop bands analogous to the zone-boundary and coupled-mode stop bands of the periodic case were predicted, and striking similarities to the periodic case were noted. Here, we extend these calculations to predict the angular distribution of phonon stop bands for a Fibonac-

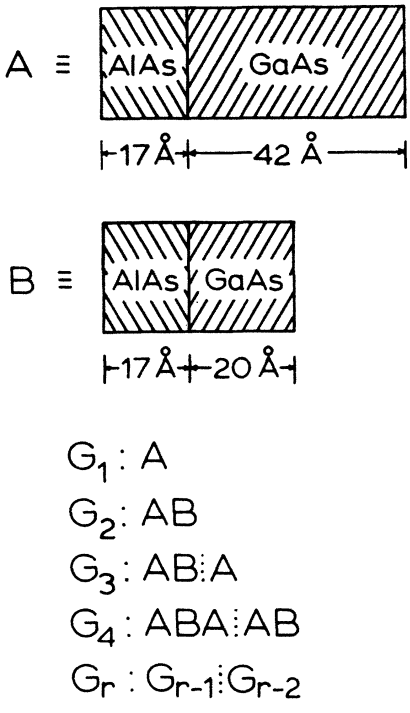

FIG. 1. The Fibonacci SL. The composition of the individual "building blocks" A and B is shown. The first four Fibonacci generations G_1, G_2, G_3, and G_4 as well as the rule to derive an arbitrary generation G_r are also indicated. (Adapted from Ref. 9.)

ci SL. Also, phonon-imaging experiments have been performed on this system with the following results: (a) ballistic transmission of 850-GHz phonons is observed through a large number of interfaces (>750), attesting to the quality of this structure; (b) attenuation associated with Bragg-like reflection is observed in all three phonon modes, as indicated by relatively sharp cutoffs in phonon intensities as the propagation angle is scanned. Due to the size of the SL layer thicknesses compared to the phonon wavelength, the observed drops in transmission correspond to higher-order Bragg reflections ($n=2,3,4$) in the periodic system.

II. THEORETICAL BACKGROUND

Figure 1 (adapted from Ref. 9) shows the layering scheme for the AlAs/GaAs Fibonacci SL created by Merlin *et al.*[9] The SL consists of individual building blocks A [(17-Å AlAs)/(42-Å GaAs)] and B [(17-Å AlAs)(20-Å GaAs)]. The sequence of A and B blocks in the SL is determined by the Fibonacci generation number r. A SL of the rth generation G_r is created by combining (i.e., concatenating or juxtaposing) the two prior generations: $G_r=G_{r-1}G_{r-2}$, where $G_1=A$ and $G_2=AB$. Thus higher generations start with the sequence $ABAABABA\cdots$. (This corresponds directly to the terms in the Fibonacci series, determined by $F_{p+1}=F_{p-1}+F_p$, where $F_0=0$ and $F_1=1$.) The ratio of the thickness of block A to that of block B is (59 Å/37 Å)$\approx\tau=(1+\sqrt{5})/2$, the golden mean.

In an infinite Fibonacci SL the structure factor which describes the phonon interference effects shows δ-function peaks at $\nu=\nu_{m,n}\equiv v(m+n\tau)/2(\tau d_A+d_B)$, where m and n are integers and v is an appropriate sound velocity.[8] This means that Bragg-like reflection of phonons occurs at frequencies $\nu=\nu_{m,n}$, and frequency gaps in the phonon-dispersion relation are created at these fre-

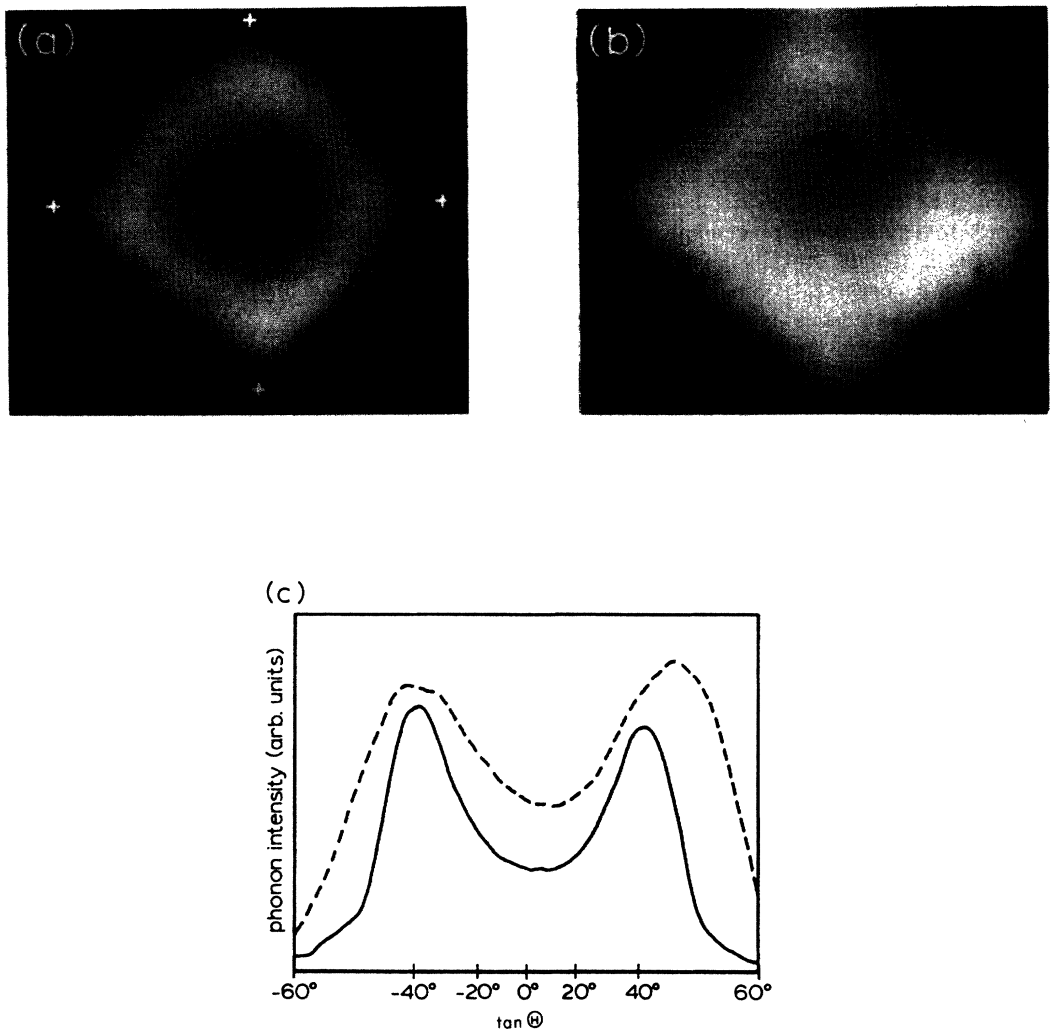

FIG. 2. (a) Experimental constant-velocity ($v=5.4$ km/s) image for L phonons propagating through a Fibonacci SL from a GaAs substrate. (b) Corresponding phonon image for the GaAs substrate alone. The center of the images is ⟨001⟩, with ⟨111⟩ directions indicated by the crosses in (a). The diagonals of the images are parallel to the (100) plane. The images span approximately ±60° left to right. (c) Scan of the phonon intensity along a line across the center of the images in (a) (solid line) and (b) (dashed line). The two curves have been arbitrarily displaced.

quencies, making a self-similar band structure.[6] In a real Fibonacci SL consisting of a finite number of layers, significant transmission dips are predicted[8] to appear at frequencies in these band gaps. The study of the structure factor for a Fibonacci SL predicts the presence of intermode Bragg-like reflections for phonons which propagate along nonsymmetry directions. That is, at oblique angles of incidence, phonons of different polarizations couple to each other. It should be noted that those phonon modes which couple together have common dips in the transmission.

As discussed in Ref. 8, the phonon transmission rate can be calculated explicitly using the transfer matrix method. We apply this method to compute the angular regions of phonon attenuation (i.e., the spatial distribution of the stop bands). Since the number of layers increases dramatically with generation number r, the numerical methods involved produce numerical inaccuracies[18] for fairly small values of r. Therefore, our calculations are restricted to SL systems with generation numbers $r \leq 7$ or 8, depending on the phonon mode involved. However, we believe that these calculations satisfactorily approximate the behavior of SL's with a larger number of layers.

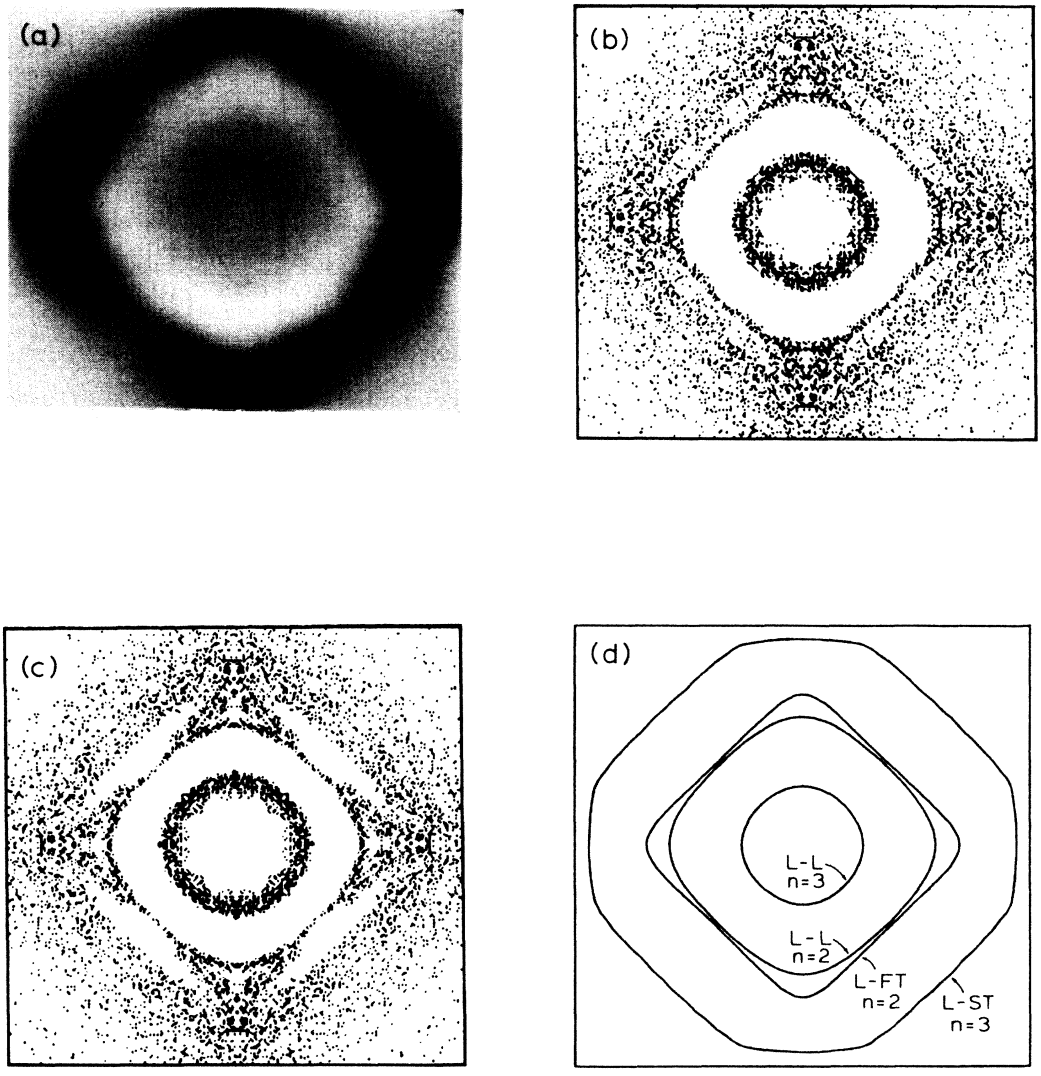

FIG. 3. (a) Difference image obtained by subtracting the substrate image in Fig. 2(b) from the SL-plus-substrate image in Fig. 2(a), shown at increased gain. The image has been quadrant averaged for a better level of signal to noise. (b) Calculated spatial dependence of L-phonon attenuation in a Fibonacci SL ($r=8$, 34 A and B blocks), $\nu=850$–900 GHz. Dark points represent phonons with a transmission rate $T<0.5$. (c) Corresponding distribution for a periodic SL with 34 blocks. (d) Maps of the single-mode and coupled-mode Bragg condition for L phonons in a periodic AlAs/GaAs SL with GaAs substrate. A phonon frequency $\nu=850$ GHz and period thickness $D=d_A+d_B=96$ Å have been assumed. The curves are labeled according to the order of reflection (n) and the mode pairs participating in the reflection. The plots in (b)–(d) span $\pm 63°$ ($\tan\Theta=\pm 2$) left to right.

III. EXPERIMENTAL RESULTS

The phonon-imaging experiments were carried out with a sample identical to that specified by Merlin *et al.* Using the method described in Fig. 1, a 13th-generation SL (377 separate A and B blocks) was fabricated with molecular-beam epitaxy (MBE) methods on a (001)-oriented GaAs substrate ~ 500 μm thick. The phonon-imaging experiments were performed in an identical manner to those described in Ref. 14, using a tunnel-junction detector with phonon cut-on frequency $\nu_c \approx 850$ GHz.

Experimental results for longitudinal (L) mode phonons are shown in Fig. 2. The image in Fig. 2(a) is for the SL-plus-substrate sample, and represents the intensity of detected phonons with velocity $v = 5.4$ km/s, i.e., L-mode phonons. For comparison, Fig. 2(b) is the L-mode image for the GaAs substrate alone. Figure 2(c) indicates the phonon intensity for horizontal scans across the center of the SL image (solid line) and substrate image (dashed line). The SL image displays a rather sharp falloff in intensity in the vicinity of $\langle 111 \rangle$ ($\Theta = 54.7°$), that is, towards the left and right edges of the scan. In addition, the intensity diminishes somewhat more sharply towards the center of the SL image than in that for the substrate.

To isolate the SL effect, the substrate image in Fig. 2(b) was subtracted from the SL-plus-substrate image in Fig. 2(a). This *difference* image is shown in Fig. 3(a) with enhanced gain. In the image, dark areas indicate attenuation by the SL. These data reveal the strong attenuation region at large angles and the somewhat weaker effect in the central region.

Figure 3(b) shows the predicted stop bands for L phonons, $\nu = 850$–900 GHz, in a Fibonacci SL ($r = 8$, 34 blocks). In this figure, the dark points represent phonons which have a transmission rate T less than 0.5. Figure 3(c) shows the same calculation for a *periodic* AlAs/GaAs SL with 34 alternating A and B blocks. It is remarkable that the two figures resemble each other closely, demonstrating that not only the *frequency* dependence[8] but also the *angular* dependence of the SL attenuation in the periodic and quasiperiodic cases is very similar.

This similarity in the angular dependence of the transmission for the two systems encourages us to compare quasiperiodic results with periodic ones in other ways. For example, spatial maps of the Bragg condition in a periodic SL can help to determine the origins of the observed stop bands. Assuming $\nu = 850$ GHz, $D = d_A + d_B = 96$ Å, the map shown in Fig. 3(d) represents the spatial dependence[14,20,21] of the Bragg condition for the L-phonon mode. This combination of ν and D means that the reflections relevant to this angular range are of order $n = 2$ or 3. Both intermode and intramode scattering processes are shown. Comparing this to the Monte Carlo images in Figs. 3(b) and 3(c), we find that the innermost ring-shaped structure centered on [100] is an intramode reflection, while the more anisotropic structures close to $\langle 111 \rangle$ are the combined effect of L-L (single-mode) and L-FT (coupled-mode)

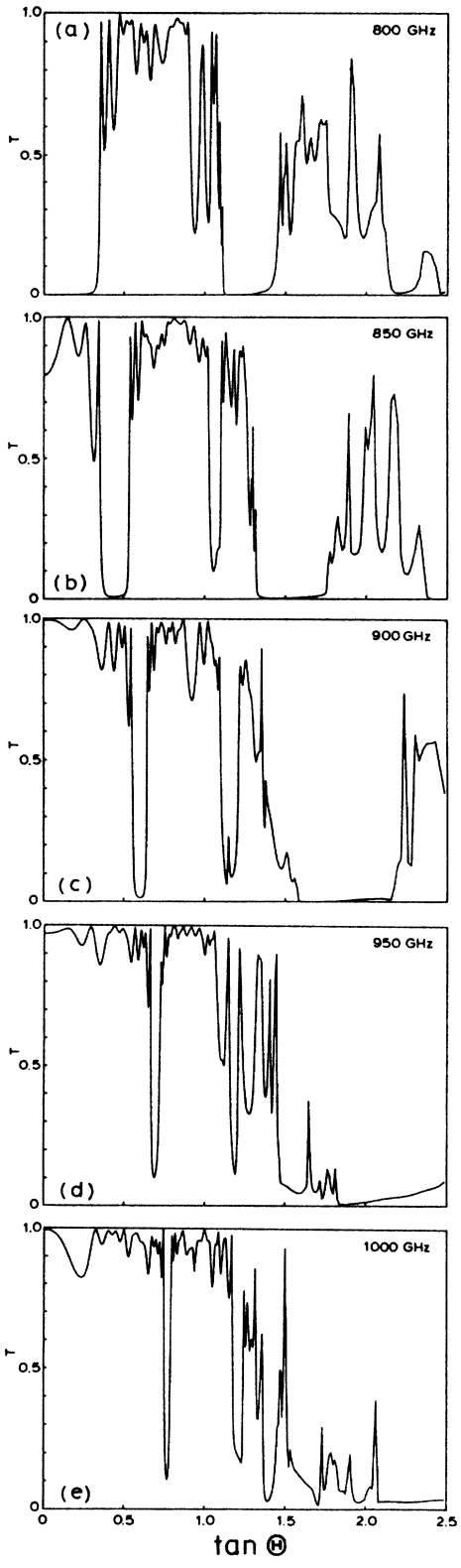

FIG. 4. Calculated transmission rate T for L phonons in a Fibonacci SL ($r = 8$) vs the real-space direction Θ. The plots were calculated assuming a fixed k-space azimuthal angle $\phi = 20°$. The plots represent the transmission rate for a phonon frequency of (a) $\nu = 800$ GHz; (b) $\nu = 850$ GHz; (c) $\nu = 900$ GHz; (d) $\nu = 950$ GHz; and (e) $\nu = 1000$ GHz.

reflections. An L-ST coupled-mode stop band appears at larger real-space angles Θ from $\langle 100 \rangle$, near the edges of the image. Examination of the difference image [Fig. 3(a)] suggests that the observed attenuation near $\langle 111 \rangle$ is likely to arise from the L-L–L-FT stop band combination. Moreover, the somewhat sharp falloff in intensity toward the center of the image could be attributed to the presence of the inner L-L stop band.

Of course, the experimental image represents a range of phonon frequencies, as determined from the gap of the superconducting tunnel-junction detector and phonon scattering in the substrate which suppresses the ballistic propagation of high-frequency phonons. Previous experiments on periodic SL's (Ref. 14) grown on GaAs substrates of similar thickness suggested that the frequency range of ballistically transmitted phonons was 850–1000 GHz. To determine more quantitatively how the transmission profile depends on phonon frequency, we have generated angular scans of the transmission rate T in an eighth-generation Fibonacci SL for phonons with $\nu = 800$, 850, 900, 950, and 1000 GHz, as shown in Figs. 4(a)–4(e). The form of the condition ($\cos\theta = n\lambda/2D$, where θ is the angle the wave vector makes with the interface normal) dictates that the stop band has a much larger width when centered on small incident angles (e.g., for 800 GHz) and becomes much sharper at large Bragg

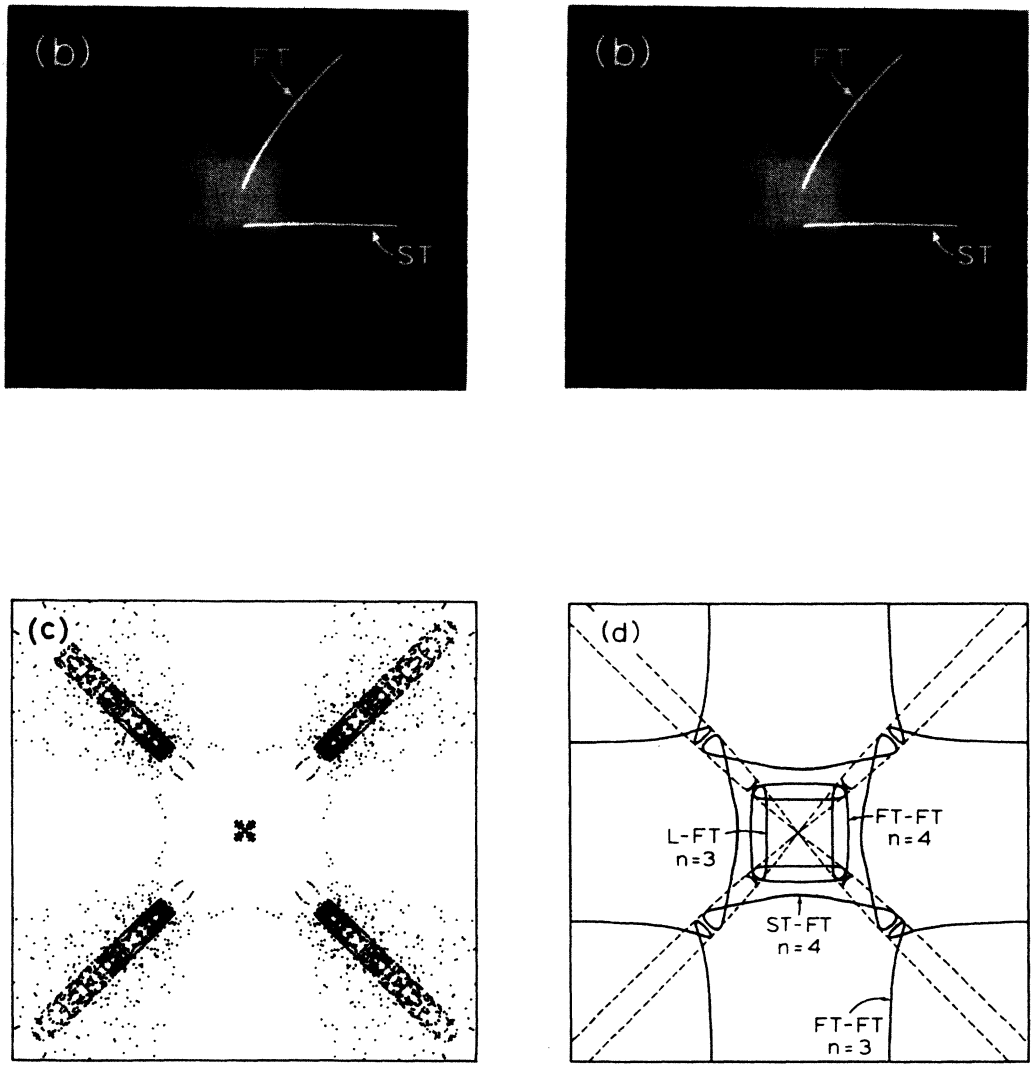

FIG. 5. (a) Constant-velocity image for FT phonons in the SL sample ($v = 3.1$ km/s). (b) Corresponding image for the substrate-only case. The images in (a) and (b) have been processed to remove a 20-μm source/detector broadening and to compensate for $1/r^2$ and $\cos\Theta$ intensity falloff. The lines labeled FT and ST refer to Figs. 6 and 8. (c) Predicted stop band distribution for FT phonons ($\nu = 850$–900 GHz) in a sixth-generation Fibonacci SL. Points represent phonons with $T < 0.5$. (d) Maps of the single-mode and coupled-mode Bragg condition for FT phonons, $\nu = 850$ GHz, $D = 96$ Å, in a periodic SL. The curves are labeled according to the mode pairs participating in the reflection. The dashed lines indicate the phonon-focusing pattern of caustics for FT phonons. The scale for each image is the same as for similar plots in previous figures.

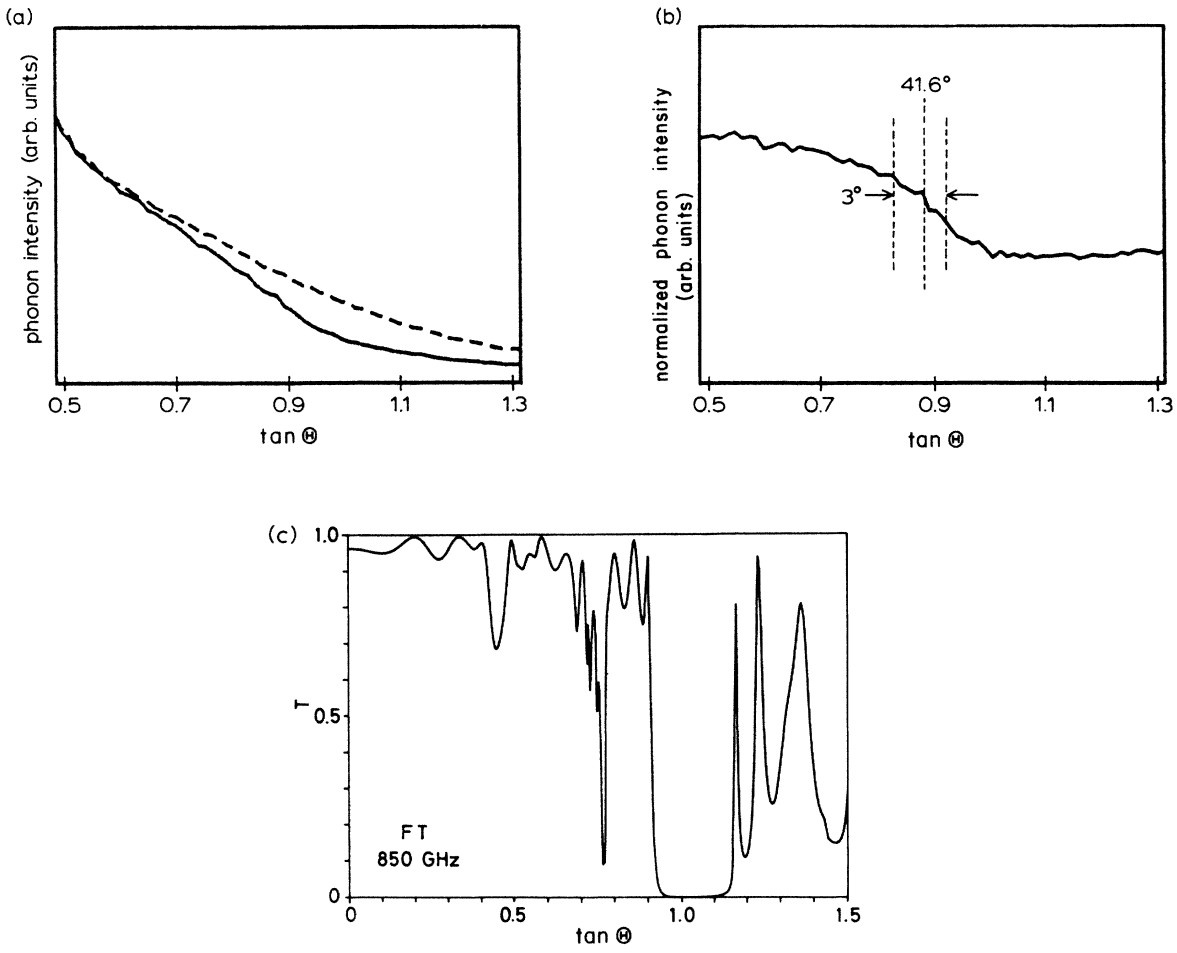

FIG. 6. (a) Transmitted phonon intensity along the FT phonon-focusing caustic for the SL sample (solid line) and substrate only (dashed line). The direction along which the curves were obtained is indicated by the line labeled FT in Fig. 5(b). (b) Normalized phonon intensity obtained by dividing the intensity in the SL sample by that in the substrate. The intensity is reduced in half at $\Theta=41.6°$, with a width of about 3°. (c) Calculated FT-mode phonon-transmission rate for a Fibonacci SL ($r=6$) as a function of real-space direction Θ along the FT caustic.

angles (e.g., for 950 and 1000 GHz), because $\Delta\theta=1/\sin\theta$. The predictions at 800 GHz seem to most closely reproduce the reduction in the central region of the experimental image.

The phonon transmission for the two transverse polarization modes also shows SL effects. Constant-velocity images for the FT mode for both the SL-plus-substrate and substrate-only samples are shown in Figs. 5(a) and 5(b), respectively. A 20-μm broadening due to detector and source size has been deconvolved from these images. The images have also been compensated for $1/r^2$ and $\cos\Theta$ dependences in the intensity. The most obvious effect of the SL is the sharp cutoff in intensity of the transverse phonons, as indicated by the arrows in Fig. 5(a). It is also interesting to note that the caustic pattern in Fig. 5(a) is relatively sharp, in spite of the fact that the phonons have propagated through 377 blocks—more than 750 interfaces, signifying a high-quality heterostructure.

Figure 5(c) shows the predicted stop band distribution for FT phonons, $\nu=850-900$ GHz, in a Fibonacci SL with $r=6$ (13 blocks). As before, phonons with a transmission rate less than 0.5 are represented. The figure indicates the presence of a stop band in the vicinity of the observed cutoff. A spatial map of the Bragg condition for FT processes, Fig. 5(d), reveals that the attenuation in this angular region arises from both a coupled-mode (ST-FT) reflection and a "normal" (FT-FT) reflection. The intensity falloff can be analyzed more quantitatively by examining the phonon intensity along the FT caustic, as indicated by the line labeled "FT" in Fig. 5(b). Figure 6(a) shows the intensity along the caustic for both the SL sample (solid line) and the substrate-only sample (dashed line). The normalized phonon intensity—i.e., the intensity in the SL-plus-substrate sample *divided* by that in the substrate alone—is shown in Fig. 6(b). A rather sharp falloff in the transmission is clearly evident. We estimate the onset of the stop band as the point where the intensity drops by a factor of 2. This occurs experimentally at $\Theta=41.6\pm1°$, with a width of about 3°, as shown. A theoretical plot of the phonon transmission factor T as a function of position along the

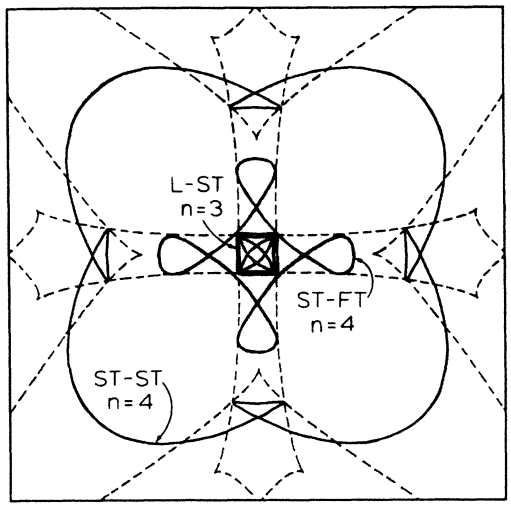

FIG. 7. Maps of the Bragg condition for ST phonons in a periodic SL with $\nu=850$ GHz, $D=96$ Å. The curves are labeled according to the mode pairs participating in the reflection. The dashed lines indicate the ST phonon-focusing caustics. The scale is the same as for corresponding plots in Fig. 3.

FT caustic is given in Fig. 6(c). Smaller dips can be seen which correspond to the FT-FT ($n=4$) and ST-FT ($n=4$) reflections. A large dropoff in intensity is observed at $\tan\Theta=0.9$, which corresponds to the FT-FT ($n=3$) stop band. This angle is almost exactly where the data of Fig. 6(b) show an intensity falloff.

The ST mode transmission also indicates an intensity cutoff. The map of the Bragg condition for the corresponding periodic SL is shown in Fig. 7. Plots of the phonon intensity along the ST caustic [indicated by the line labeled "ST" in Fig. 5(b)] and the normalized phonon intensity are shown in Figs. 8(a) and 8(b), respectively. These scans indicate a noticeable ST cutoff occurring experimentally at $\Theta=34.5\pm1°$. The Bragg map indicates an ST-FT stop band in the range $\Theta\approx21°-38°$. Thus, it seems likely that the observed ST attenuation can be attributed to the same ST-FT stop band responsible for the FT mode attenuation.

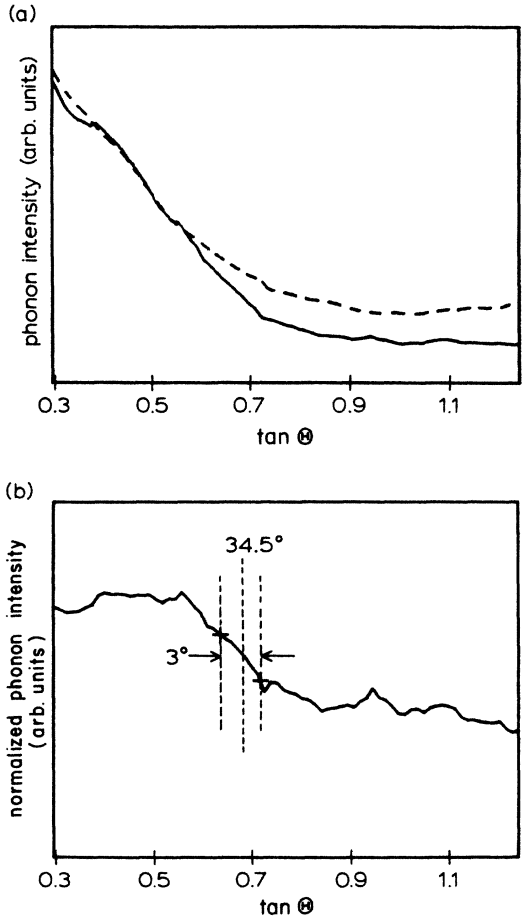

FIG. 8. (a) Transmitted phonon intensity along the ST phonon-focusing caustic. The direction along which the curves were obtained is indicated by the line labeled ST in Fig. 5(b). Transmission for the SL sample (solid line) and substrate only (dashed line) are both shown. (b) Normalized phonon intensity obtained by dividing the phonon intensity in the SL sample by that in the substrate sample. The intensity is decreased by a factor of 2 at $\Theta=34.5°$, with a width of about 3°.

IV. CONCLUSIONS

Phonon-imaging experiments of the acoustic-phonon transmission through a quasiperiodic superlattice indicate attenuation due to Bragg-like reflections for all three polarization modes. Calculations presented here are in reasonable agreement with the experimental results. The calculations are based on estimates of the SL elastic constants and ignore dispersive effects,[22] which in the present case amount to approximately a 10% correction in the phonon velocity for the transverse modes. Some experimental uncertainties exist in the phonon-frequency distribution and SL layer thicknesses. Nevertheless, it is clear that in a Fibonacci SL, sharp angular variations in the transmitted phonon intensity can be observed. The attenuation is associated with Bragg-like reflection processes, and is quite similar to the periodic case in its angular and frequency dependence.

ACKNOWLEDGMENTS

We thank F. Nori and R. Merlin for suggesting these experiments and coordinating the collaboration between the University of Illinois and Max-Planck-Institut research groups. Support for the University of Illinois work was provided by National Science Foundation (NSF) Grant No. DMR-86-12860. One of us (S.T.) acknowledges a travel grant by the Department of Education, Science, and Culture of Japan.

*Permanent address: Department of Engineering Science, Hokkaido University, Sapporo 060, Japan.

[1]D. Shechtman, I. Blech, D. Gratias, and J. W. Cahn, Phys. Rev. Lett. **53**, 1951 (1984); for a review, see D. R. Nelson and B. I. Halperin, Science **229**, 233 (1950).

[2]D. Levine and P. J. Steinhardt, Phys. Rev. Lett. **53**, 2477 (1984); Phys. Rev. B **34**, 596 (1986).

[3]J. P. Lu, T. Odagaki, and J. L. Birman, Phys. Rev. B **33**, 4809 (1986).

[4]M. Kohmoto and J. R. Banavar, Phys. Rev. B **34**, 563 (1986).

[5]M. Kohmoto, Phys. Rev. B **34**, 5043 (1986).

[6]F. Nori and J. P. Rodriguez, Phys. Rev. B **34**, 2207 (1986).

[7]R. K. P. Zia and W. J. Dallas, J. Phys. A **18**, L341 (1985).

[8]S. Tamura and J. P. Wolfe, Phys. Rev. B **36**, 3491 (1987).

[9]R. Merlin, K. Bajema, R. Clarke, F.-Y. Juang, and P. K. Bhattacharya, Phys. Rev. Lett. **55**, 1768 (1985).

[10]J. Todd, R. Merlin, R. Clarke, K. M. Mohanty, and J. D. Axe, Phys. Rev. Lett. **57**, 1157 (1986).

[11]M. W. C. Dharma-wardana, A. H. MacDonald, D. J. Lockwood, J.-M. Barbibeau, and D. C. Houghton, Phys. Rev. Lett. **58**, 1761 (1987).

[12]V. Narayanamurti, H. L. Störmer, M. A. Chin, A. C. Gossard, and W. Wiegmann, Phys. Rev. Lett. **43**, 2012 (1979).

[13]O. Koblinger, J. Mebert, E. Dittrich, S. Döttinger, W. Eisenmenger, P. V. Santos, and L. Ley, Phys. Rev. B **35**, 9372 (1987).

[14]D. C. Hurley, S. Tamura, J. P. Wolfe, and H. Morkoc, Phys. Rev. Lett. **58**, 2446 (1987); S. Tamura, D. C. Hurley, and J. P. Wolfe, Phys. Rev. B (to be published).

[15]P. V. Santos, J. Mebert, O. Koblinger, and L. Ley, Phys. Rev. B **36**, 1306 (1987).

[16]R. E. Camley, B. Djarfari-Rouhani, L. Dobryzynski, and A. A. Maradudin, Phys. Rev. B **27**, 7318 (1983).

[17]M. Babiker, D. R. Tilley, E. L. Albuquerque, and C. E. T. Goncalves da Silva, J. Phys. C **18**, 1269 (1985).

[18]M. J. Kelly, J. Phys. C **18**, 5963 (1985).

[19]S. Tamura and J. P. Wolfe, Phys. Rev. B **35**, 2528 (1987), and references therein.

[20]The phonon velocities in the SL were calculated using an effective density and effective elastic constants, obtained by weighting the AlAs and GaAs values by the relative A and B layer thicknesses [i.e., $C_{\text{eff}}=(34/96)C_{\text{AlAs}}+(62/96)C_{\text{GaAs}}$]. For numerical values, see S. Adachi, J. Appl. Phys. **58**, R3 (1985).

[21]Tamura and Wolfe's work (Ref. 8) indicates that the exact condition for reflection in the Fibonacci SL can be obtained by substituting the quantities $(m+n\tau)$ and (τd_A+d_B) for n and D in the periodic Bragg condition.

[22]G. A. Northrop, S. E. Hebboul, and J. P. Wolfe, Phys. Rev. Lett. **55**, 95 (1985).

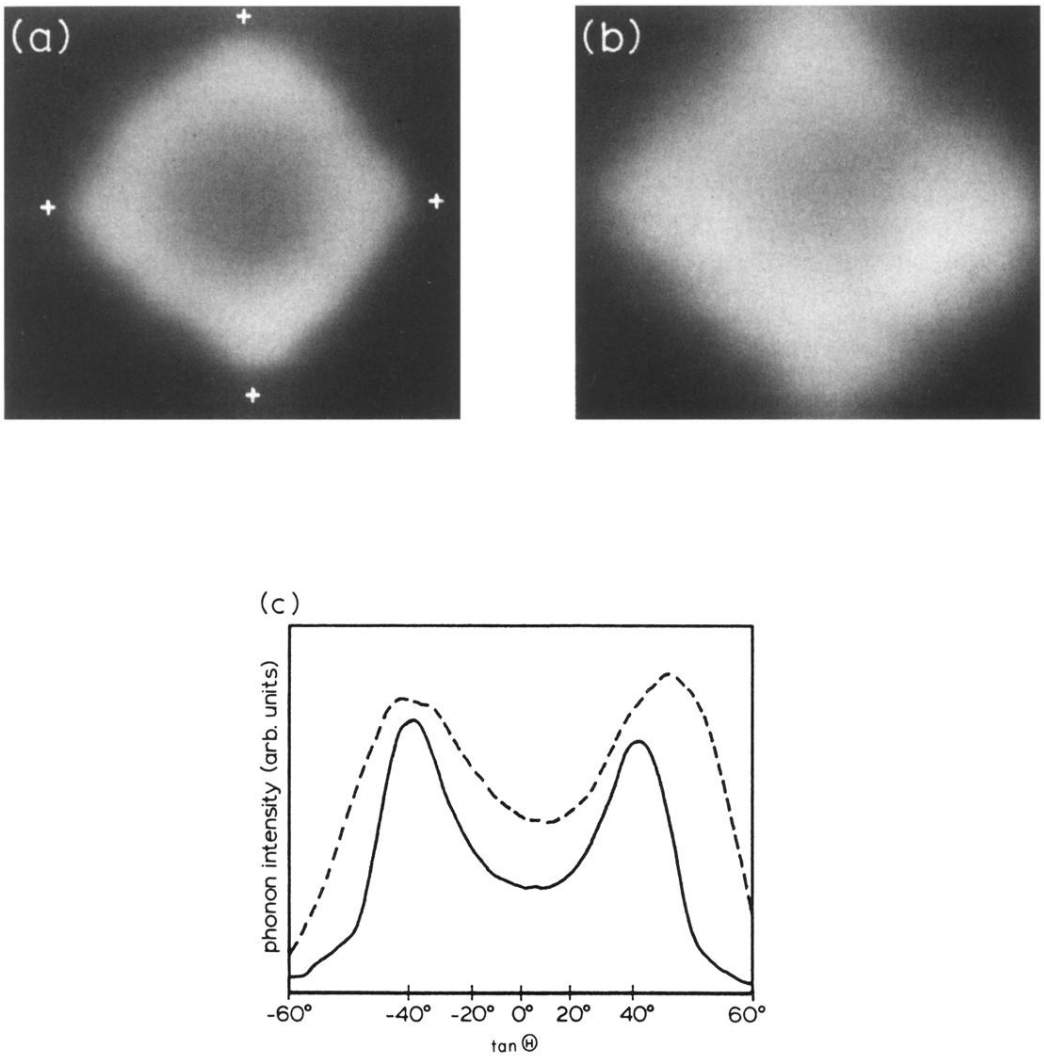

FIG. 2. (a) Experimental constant-velocity ($v = 5.4$ km/s) image for L phonons propagating through a Fibonacci SL from a GaAs substrate. (b) Corresponding phonon image for the GaAs substrate alone. The center of the images is ⟨001⟩, with ⟨111⟩ directions indicated by the crosses in (a). The diagonals of the images are parallel to the (100) plane. The images span approximately ±60° left to right. (c) Scan of the phonon intensity along a line across the center of the images in (a) (solid line) and (b) (dashed line). The two curves have been arbitrarily displaced.

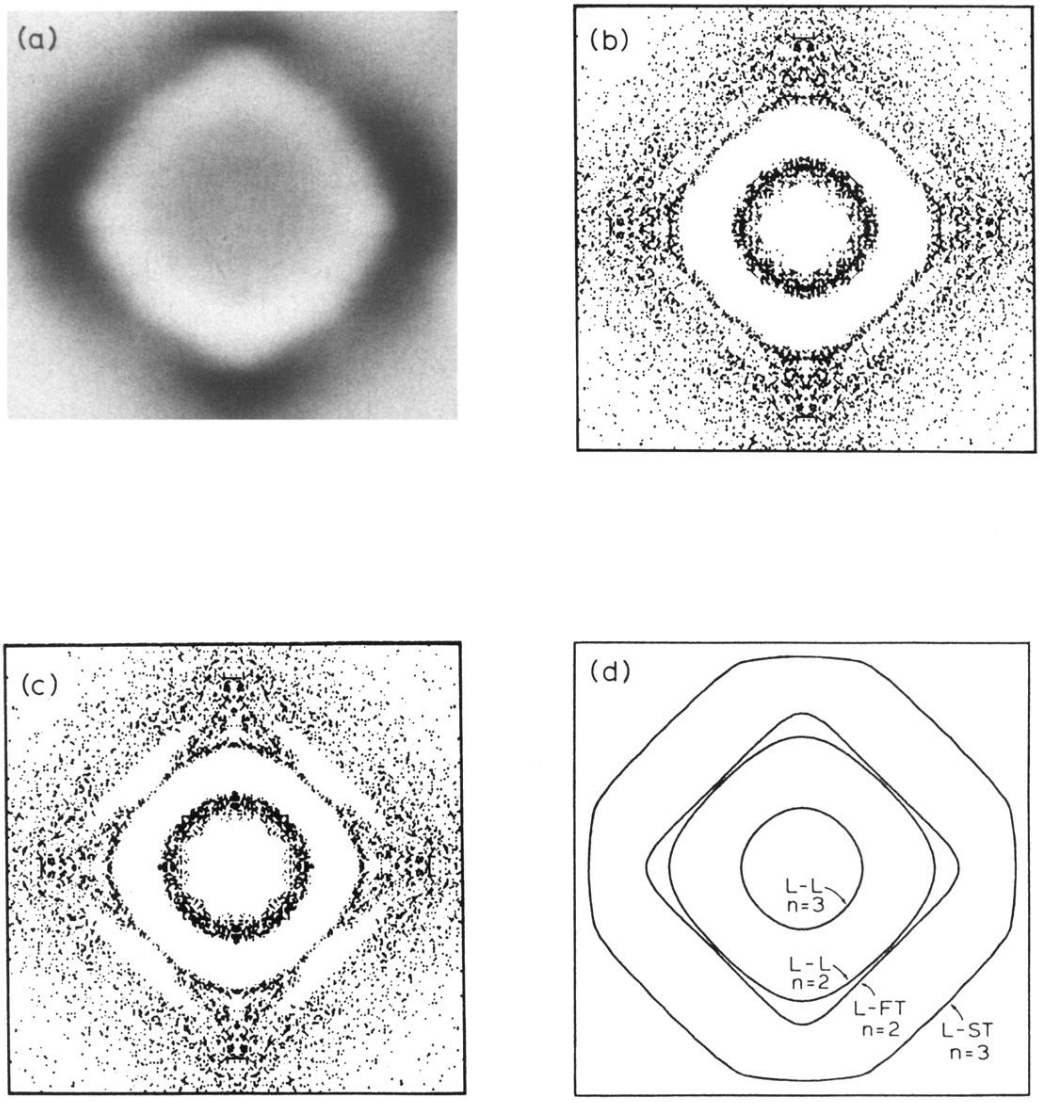

FIG. 3. (a) Difference image obtained by subtracting the substrate image in Fig. 2(b) from the SL-plus-substrate image in Fig. 2(a), shown at increased gain. The image has been quadrant averaged for a better level of signal to noise. (b) Calculated spatial dependence of L-phonon attenuation in a Fibonacci SL ($r=8$, 34 A and B blocks), $\nu=850$–900 GHz. Dark points represent phonons with a transmission rate $T<0.5$. (c) Corresponding distribution for a periodic SL with 34 blocks. (d) Maps of the single-mode and coupled-mode Bragg condition for L phonons in a periodic AlAs/GaAs SL with GaAs substrate. A phonon frequency $\nu=850$ GHz and period thickness $D=d_A+d_B=96$ Å have been assumed. The curves are labeled according to the order of reflection (n) and the mode pairs participating in the reflection. The plots in (b)–(d) span $\pm 63°$ ($\tan\Theta=\pm 2$) left to right.

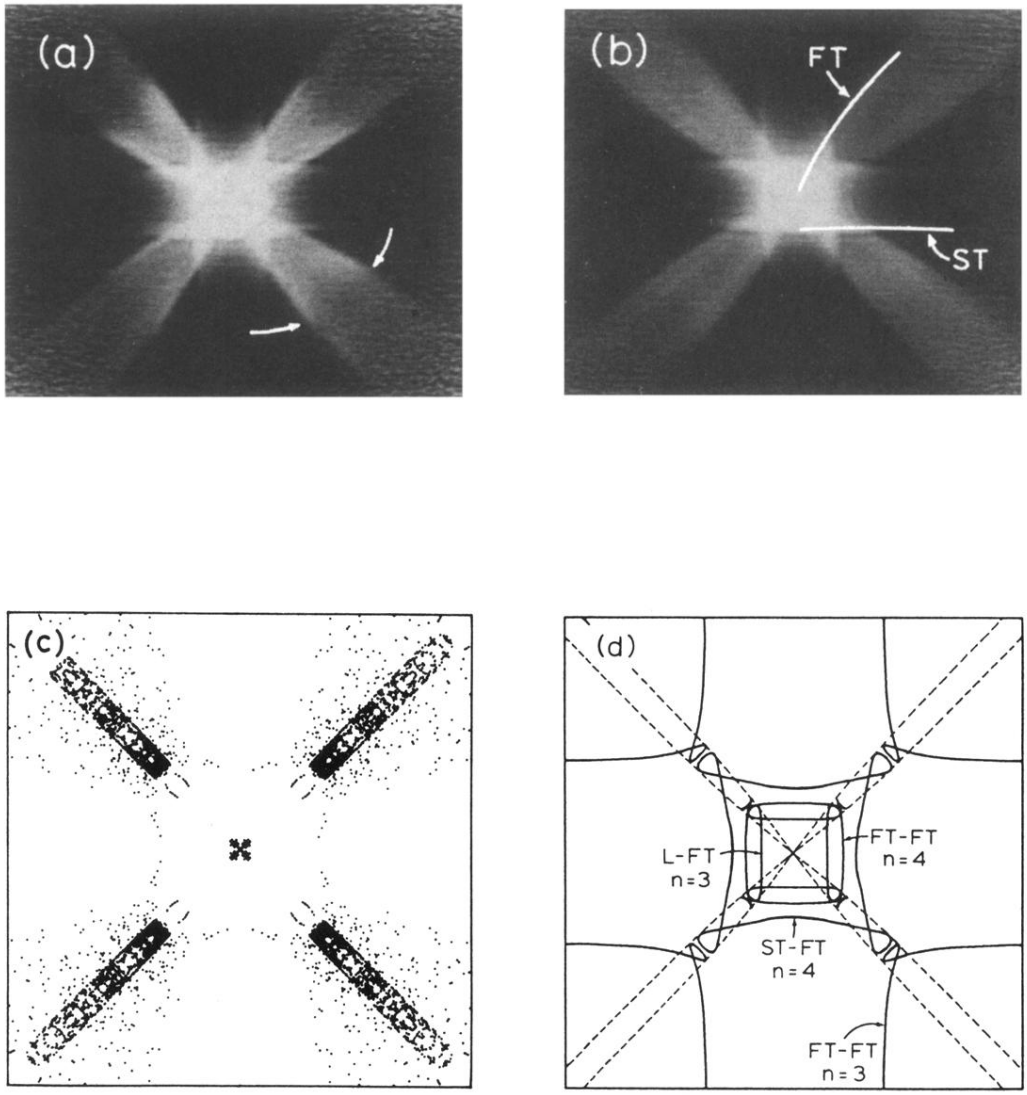

FIG. 5. (a) Constant-velocity image for FT phonons in the SL sample ($v = 3.1$ km/s). (b) Corresponding image for the substrate-only case. The images in (a) and (b) have been processed to remove a 20-μm source/detector broadening and to compensate for $1/r^2$ and cosΘ intensity falloff. The lines labeled FT and ST refer to Figs. 6 and 8. (c) Predicted stop band distribution for FT phonons ($\nu = 850$–900 GHz) in a sixth-generation Fibonacci SL. Points represent phonons with $T < 0.5$. (d) Maps of the single-mode and coupled-mode Bragg condition for FT phonons, $\nu = 850$ GHz, $D = 96$ Å, in a periodic SL. The curves are labeled according to the mode pairs participating in the reflection. The dashed lines indicate the phonon-focusing pattern of caustics for FT phonons. The scale for each image is the same as for similar plots in previous figures.